Published in final edited form as:
Neuron. 2007 December 20; 56(6): 1061–1075.

Long-term potentiation in rat hippocampal neurons is accompanied by spatially widespread changes in intrinsic oscillatory dynamics and excitability

Rishikesh Narayanan and **Daniel Johnston**
Center for Learning and Memory, The University of Texas at Austin, Austin, TX78712

SUMMARY

Oscillations in neural activity are a prominent feature of many brain states. Individual hippocampal neurons exhibit intrinsic membrane potential oscillations and intrinsic resonance in the theta frequency range. We found that the subthreshold resonance frequency of CA1 pyramidal neurons was location-dependent, varying more than threefold between the soma and the distal dendrites. Furthermore, activity- and NMDA-receptor-dependent long-term plasticity increased this resonance frequency through changes in *h*-channel properties. The increase in resonance frequency and an associated reduction in excitability were nearly identical in the soma and the first 300 μm of the apical dendrites. These spatially widespread changes accompanying long-term synaptic potentiation also reduced the neuron's ability to elicit spikes evoked through a non-potentiated synaptic pathway. Our results suggest that the frequency response of these neurons depends on the dendritic location of their inputs and that activity can regulate their response dynamics within an oscillating neural network.

Keywords

hippocampus; homeostasis; intrinsic oscillations; I_h; frequency selectivity; activity-dependent plasticity; membrane resonance

INTRODUCTION

Membrane potential oscillations (MPOs) in neurons are thought to be involved in memory encoding and network synchronization (Alonso and Garcia-Austt, 1987; Bland and Colom, 1993; Buzsaki, 2002; Engel et al., 2001; O'Keefe and Burgess, 2005). Among the roles ascribed to MPOs are augmentation of synaptic inputs that are in synchrony with MPOs (Volgushev et al., 1998), frequency selectivity (Hutcheon and Yarom, 2000; Strohmann et al., 1994), precision of action potential timing (Schaefer et al., 2006), and genesis of network rhythms (Alonso and Garcia-Austt, 1987; Buzsaki, 2002). Although oscillations in nervous systems have been studied for these and various other physiological roles they play (Buzsaki, 2002; Engel et al., 2001; Marder and Calabrese, 1996; Oestreich et al., 2006; Ramirez et al., 2004; Steriade and Timofeev, 2003), plasticity in intrinsic subthreshold oscillatory dynamics has not been explored.

Corresponding Author: Daniel Johnston, Ph.D., Center for Learning and Memory, The University of Texas at Austin 1, University Station Stop, C7000, Austin, TX 78712–0805, USA., e-mail: djohnston@mail.clm.utexas.edu, Phone: 512–232–6564, Fax: 512–475–8000.

Intrinsic MPOs are mediated by voltage-gated ion channels (Hutcheon and Yarom, 2000; Llinas, 1988) and are dependent on two classes of ion-channel conductances (Hutcheon et al., 1996; Hutcheon and Yarom, 2000): (i) a resonating conductance, which forms the substrate for oscillations, determines the frequency of oscillations, governs the frequency-dependent response of the neuron, and sustains resonance on its own; and (ii) an amplifying conductance, which governs the amplitude of oscillations. NMDA-type glutamate receptors and persistent sodium (NaP) channels have been suggested to act as amplifying conductances, while the *M*-type K^+ and hyperpolarization-activated *h* conductances act as resonating conductances (Hu et al., 2002; Hutcheon and Yarom, 2000). As a direct consequence of the presence of a resonating conductance, neurons endowed with intrinsic oscillations exhibit resonance, which has been used as a tool to assess their intrinsic oscillatory dynamics (Hu et al., 2002; Hutcheon et al., 1996; Hutcheon and Yarom, 2000; Leung and Yu, 1998).

In the hippocampus, MPOs during the waking state are in the theta frequency range of 3–10 Hz (Buzsaki, 2002; O'Keefe and Burgess, 2005). While theta oscillations in hippocampus are due to network interactions among pyramidal and inter-neurons, it is also clear that individual neurons are capable of sustaining intrinsic oscillations and that the intrinsic properties of these neurons play a prominent role in the network behavior (Buzsaki, 2002; Leung and Yim, 1991; O'Keefe and Burgess, 2005). Hippocampal CA1 pyramidal neurons exhibit subthreshold membrane potential oscillations (Leung and Yu, 1998; Leung and Yim, 1991). These neurons are endowed with the two resonating currents, I_h and I_M, mediating resonance at hyperpolarized and depolarized voltages, respectively, with I_{NaP} acting as a putative amplifying current (Hu et al., 2002; Leung and Yim, 1991).

In this study, we investigated the intrinsic subthreshold membrane resonance of CA1 pyramidal neurons and found that it was not a fixed property, but instead was highly variable depending on the membrane potential, spatial location in the dendrites, and activity. The frequency of the intrinsic resonance varied more than three-fold between the soma and distal regions of the dendrites, and was in accordance with the reported change in *h*-channel density (Lorincz et al., 2002; Magee, 1998). Furthermore, the induction of activity-dependent, long-term plasticity increased the resonant frequency and reduced input resistance by similar amounts in the dendrites on the apical trunk within stratum radiatum. Surprisingly, in striking contrast to the localized nature of changes in the A-type potassium current (Frick et al., 2004), we found that this plasticity is spatially widespread even when it accompanies pathway-specific long-term synaptic potentiation (LTP). Employing computational analyses, we argue that such spatially widespread changes in resonance frequency and input resistance cannot be realized through locally confined changes in I_h, but require changes in *h*-channel properties to span a broad region of the dendritic tree. Our results suggest that these neurons can act as stimulus-dependent matched filters for spatially separated inputs, regulated by prior history of activity converging onto the neuron. Further, this spatially widespread expression of plasticity supports the role for I_h as a homeostatic mechanism counterbalancing the positive feedback associated with Hebbian plasticity (Bienenstock et al., 1982; Turrigiano and Nelson, 2000).

RESULTS

Resonance is the increase in the amplitude of oscillations of a system exposed to a periodic force whose frequency is equal to or very close to the natural frequency of the system. In neurons, this natural frequency corresponds to that of membrane potential oscillations (MPOs), and can be measured as the frequency at which the neuron elicits the maximal voltage response to sinusoidal current injections of various frequencies. Alternately, a sinusoidal current stimulus of constant amplitude, with frequency linearly spanning a given range over time, can be used as a tool to measure resonance properties of a neuron. Such a sinusoid has been termed a ZAP stimulus, which stands as an acronym for impedance amplitude profile (see Fig. S1)

(Hutcheon and Yarom, 2000). In this study, we use the ZAP stimulus to characterize and assess plasticity in intrinsic membrane resonance of soma and dendrites in CA1 pyramidal neurons.

Resonance frequency in dendrites increases with distance from soma

Subthreshold resonance depends on *h*-channels (Hu et al., 2002), and *h*-channel density in apical dendrites increases with distance from the soma (Lorincz et al., 2002; Magee, 1998). Therefore, we tested whether this translates to location-dependence of resonance properties in the dendrites. We obtained responses of the soma and the dendrites to the ZAP20 current stimulus (Fig. S1A). Our results, binned into six different distances and measured at five different subthreshold voltages, show that irrespective of distance from the soma, resonance frequency, f_R (in the voltage range −75 mV to −55 mV), increased monotonically with hyperpolarization (Fig. 1B; *e.g.*, Soma: 1.78 ± 0.21 Hz at −55mV to 4.92 ± 0.44 Hz at −75 mV; 300 μm: 3.63 ± 1.28 Hz at −55 mV to 11.10 ± 0.1 Hz at −75 mV). However, f_R in the dendrites increased considerably with increasing distance from the soma (Fig. 1C). f_R at −65 mV varied from about 3 Hz in the soma to 9 Hz in a dendrite 300 μm from the soma. A single exponential was used to fit the experimental f_R vs. distance curves with a τ of about 75 μm, although sigmoidal functions could also be used (Fig. S2A), especially because at rest, dendritic f_R does not change much up to around 250 μm from the soma, while displaying a steep increase beyond that (Fig. S2A-B). Resonance strength (Q) also increased with hyperpolarization (Fig. 1D), and with distance from the soma (Fig. 1E). Consistent with previous studies (Magee, 1998), input resistance ($\bar{R}_{in}$)decreased with hyperpolarization (Fig. 1F) and with distance from soma (Fig. 1G).

Subthreshold resonance is dependent on *h*-channels

Although the density of *h*-channels (Lorincz et al., 2002; Magee, 1998) and resonance properties increase with distance from the soma, we tested directly whether f_R, in fact, depended on I_h. We pretreated slices for five minutes with 100 μM ZD7288 and assessed resonance properties (Fig. S3) at various locations along the somato-apical trunk (Fig. 2A), without adding ZD7288 to the recording solutions. We found that f_R, along the entire measured range of voltages and distances, was below 1 Hz (Fig. 2B-C), suggesting that blocking I_h abolished resonance in the subthreshold voltage range. This was corroborated by measurements of Q, all of which were just above the theoretical minimum of unity across the measured voltage range (Fig. 2D) and distance (Fig. 2E). There was a reduction in ($\bar{R}_{in}$) with hyperpolarization (Fig. 2F), although it remained almost constant as a function of distance (Fig. 2G). Pretreatment with 20 μM ZD7288 led to identical results with respect to all parameters (data not shown).

Resonance observed at more depolarized voltages has been reported to be mediated by I_M (Hu et al., 2002). We thus tested the effects of carbachol on membrane resonance and found that it blocked resonance at depolarized potentials, but had little effect on resonance at hyperpolarized potentials (Fig. S4), consistent with CA1 neurons exhibiting two forms of resonance (Hu et al., 2002).

Activity-dependent plasticity of resonance properties

It has recently been demonstrated in CA1 pyramidal neurons that theta burst firing (TBF) results in a reduction of excitability through increases in I_h (Fan et al., 2005). Based on the results shown above, we postulated that an activity-dependent increase in I_h should also lead to increases in both f_R and Q. To test this directly, we induced activity-dependent plasticity in I_h using the TBF protocol (Fan et al., 2005) and measured resonance properties through the course of the experiment (Fig. 3).

Typical somatic responses to the ZAP15 stimulus (Fig. S5B) before and 40 minutes after TBF illustrate an increase in f_R (Fig. 3B-C). When the experiment was repeated over a number of

cells, there was a significant increase in f_R (Fig. 3D) accompanied by a significant reduction in R_{in} (Fig. S5). Consistent with earlier observations (Fan et al., 2005), there was also a significant 3.25 mV depolarizing shift in resting membrane potential (RMP, $p<0.001$).

NMDA receptors mediated the resonance plasticity

Because previous results demonstrate that the TBF-induced plasticity in excitability is dependent on the activation of NMDA receptors (Fan et al., 2005), we tested whether the plasticity in resonance properties was also dependent on these receptors. We found that bath application of the NMDAR antagonists suppressed TBF-induced depolarization of the RMP, increase in f_R (Fig. 3E, 3H), reduction in $\bar{R}_{in}$ (Fig. 3F), reduction in firing frequency (Fig. S5), and increases in percentage sag and Q (Fig. 3I). Changes in f_R and $\bar{R}_{in}$ were strongly correlated (Fig. 3G), suggesting a common mechanism underlying changes in both the parameters; in contrast, changes during the experiments with NMDAR antagonists hovered around their respective baselines (Fig. 3G).

Plasticity in excitability and resonance extends to dendrites

Although TBF induced plasticity in excitability and resonance as measured at the soma (Fig. 3), it is not known if this extends to plasticity in dendrites. A direct way to address this is to measure changes in excitability and resonance across the dendritic tree, using plasticity induced through TBF of axo-somatically initiated action potentials driven by antidromic stimulation (Frick et al., 2004). We term this form of theta burst firing through antidromic stimulation as antidromic TBF, or ATBF (Fig. S6B).

Following ATBF, there was a significant depolarizing shift in the RMP of ~3 mV at all locations measured. The time courses of reduction in $\bar{R}_{in}$ (Fig. 4B) and increase in f_R (Fig. 4C) were nearly identical at all three locations along the somato-apical trunk. The changes in f_R and $\bar{R}_{in}$ were strongly correlated for all three locations (Fig. 4D), again suggesting a possible common mechanism underlying changes in both the parameters across the dendritic tree. Further, the percentage of changes in all measured parameters were nearly identical for all locations in the dendrites (Fig. 4E). Finally, the reduction in R_{in} also translated into a reduction in firing frequency of action potentials elicited in response to a range of local current injections, and was observed in all three locations (Fig. 4F–I). Together, these suggest that activity-dependent plasticity in excitability and resonance were nearly identical across the somato-apical trunk.

LTP is accompanied by spatially widespread changes in excitability and resonance

Because there have been reports of localized changes in certain ion channels accompanying LTP (Frick et al., 2004), we asked if plasticity evoked by theta burst firing pattern would remain spatially widespread (Fig. 4) if this pattern is paired with orthodromic stimulation to induce LTP. A direct way to address this is to measure changes in excitability and resonance across the dendritic tree, using plasticity induced through pairing of antidromic stimulation with orthodromic stimulation (Frick et al., 2004). We term this form of theta burst pairing (TBP) involving antidromic stimulation as antidromic TBP, or ATBP (Fig. S7B).

ATBP led to robust LTP as measured across the somato-apical trunk (Fig. 5B). Further, all the changes that were observed with ATBF (Fig. 4) were also obtained with ATBP (Fig. 5). Specifically, across the somato-apical trunk, a ~3 mV shift in RMP, a near-identical reduction in $\bar{R}_{in}$ (Fig. 5C), a near-identical increase in f_R (Fig. 5D), correlated time courses of $\bar{R}_{in}$ and f_R (Fig. 5E), increases in Q and sag (Fig. 5F) and a reduction in action potential firing frequency (Fig. 5G–I) were observed with ATBP as well. Thus, LTP-associated plasticity in resonance and excitability were spatially widespread.

LTP is accompanied by non-local reduction in temporal summation

We next performed experiments to test if temporal summation, a physiological measurement modulated by I_h (Magee, 1998), also undergoes non-local plasticity with LTP. First, we found that temporal summation was reduced across the dendritic tree by recording α-EPSP summation at various locations along the somato-apical trunk before and after ATBP (Fig. 6A–C). Second, we performed two-pathway LTP experiments (Fig. 6D–F) and showed that while LTP was pathway-specific (Frick et al., 2004), temporal summation of evoked EPSPs on the non-LTP pathway reduced after TBP (Fig. 6G–H). We also showed that the number of spikes evoked through temporal summation was reduced after TBP (Fig. 6I–J), confirming with α-EPSP summation that these changes in evoked summation were due to changes in postsynaptic components (Fig. 6G–J). Thus, even though LTP induced through TBP was local and input-specific, the associated reduction in temporal summation and evoked action potentials was not local.

Resonance properties are directly related to I_h

Although the results described above strongly support a role for I_h in subthreshold resonance, the data did not address whether there is a direct, graded relationship between *h*-conductance and resonance properties. To assess this, we constructed a simple, single-compartment model with I_h as the only active current (Fig. S11). When the maximal density of *h*-conductance, $\bar{g}_h$, was set to zero, the response of the model (Fig. 7A; $\bar{g}_h$=0 μS/cm^2) to the ZAP20 stimulus (Fig. S1A) resembled that obtained experimentally with ZD7288 (Fig. 2 and Fig. S3A). The corresponding impedance amplitude profile (Fig. 7B; $\bar{g}_h$=0 μS/cm^2), with its peak around zero frequency, also was similar to the one obtained with ZD7288 (Fig. S3B). This is to be expected because without I_h, the model acts as a passive, parallel resistor-capacitor circuit.

When $\bar{g}_h$ was increased (Fig. 7A), the impedance amplitude peak shifted towards non-zero frequency values (Fig. 7B), confirming that I_h is a resonating conductance (Hu et al., 2002;Hutcheon et al., 1996;Hutcheon and Yarom, 2000). Importantly, we found that both f_R and Q increased monotonically with the increase in $\bar{g}_h$, supporting the notion of a direct, graded relationship between *h*-conductance and resonance properties (Fig. 7C; also see (Hutcheon et al., 1996) for a rigorous mathematical analysis of a similar model).

To assess the dependence of f_R and Q on other parameters related to the *h*-conductance, we set $\bar{g}_h$ to 6 mS/cm^2 so that f_R was ~5 Hz at −65mV. To test the effect of a shift in the I_h activation curve on resonance properties, we plotted both f_R and Q as functions of $V_{1/2}$ of the *h*-conductance (Fig. 7D) and found that both parameters exhibited a bell-shaped dependence on $V_{1/2}$, with their peaks occurring around the voltage at which the measurements were made (−65 mV). Further, simulations were in agreement with our experimental results of an increase in both f_R and Q in the −55 mV to −75 mV range of membrane voltage, while also bringing out a bell-shaped curve for the f_R vs. V_m relationship with a peak around the $V_{1/2}$ of the I_h activation curve (Fig. 7E; default $V_{1/2}$=−82 mV).

These simulations, along with the results obtained with ZD7288 (Fig. 2), argue that the distance-dependent increases in f_R (Fig. 1) are due to an increase in I_h and not due an increase in a leak conductance. The arguments follow from the observations that there was no gradient of R_{in} (or f_R) after blocking I_h (Fig. 2C & 2G), R_{in} and f_R were functions of membrane potential in accordance with the voltage dependence of I_h (Figs. 1, S1C, S3B and 7), and Q increased with distance (Fig. 1E), which is a theoretical prediction for the role of I_h and opposite to what would occur from an increase in leak conductance (Fig. S11D). Finally, the increase in Q with TBF/TBP (Fig. 3–6), accompanied by a reduction in impedance amplitude at lower but not at higher frequencies (Fig. 3C; Fig. 7B; Fig. S7G) suggest that an increase in I_h is responsible for

the activity-dependent increase in f_R (also see Fig. S11), which conforms to earlier findings on increase in I_h with TBF/TBP (Fan et al., 2005).

Gradient in resonance frequency matches measured gradient in *h*-channel density

Although there is an increase in both the density of *h*-channels (Lorincz et al., 2002; Magee, 1998) and f_R with distance (Fig. 1C), a block of resonance by ZD7288 (Fig. 2), and a direct relationship between resonance and I_h (Fig. 7), we do not know if a gradient in channel density (Lorincz et al., 2002; Magee, 1998) can account for the experimentally measured gradient in resonance properties (Fig. 1C). To address this question, we built a multi-compartmental model with a morphologically realistic three-dimensional reconstruction of a CA1 pyramidal neuron (Fig. 8A). The only active conductance we added to the model was the *h*-conductance. In deciding on the density gradient of *h*-conductance across the dendritic tree, we took into account the following experimental observations: (i) a 55–70 fold increase in channel density in distal dendrites with respect to that at the soma; and (ii) a 13–25 fold increase in channel density in distal dendrites when compared to that at proximal dendrites (Lorincz et al., 2002). Quantitatively assessing the effect of various density gradients on f_R (Fig. S12) and taking into account these experimental measurements, we found that a $\bar{g}_h$ profile that matched the experimental measurements of f_R occurred when we used a sigmoid (80-fold increase from the soma to the distal-most point on the apical trunk; Fig. 8B):

$$\bar{g}_h = 34\left(1 + \frac{100}{1 + \exp\left(\frac{380 - d_R}{34}\right)}\right)\ \mu\text{S/cm}^2$$

, where d_R is the radial distance (in μm) of the dendritic location from the soma. Along the somato-apical trunk, $V_{1/2}$ was −82 mV for $d_R \leq 100$ μm, linearly varied from −82 mV to −90 mV for $100 \leq d_R \leq 300$ μm, and −90 mV for $d_R > 300$ μm (Magee, 1998). The basal dendrites had somatic $\bar{g}_h$ and $V_{1/2}$, and apical obliques had the same $\bar{g}_h$ and $V_{1/2}$ as the trunk compartment from which they originate (Poirazi et al., 2003). We found that f_R values obtained from simulations performed with this profile matched the experimental values of f_R quite well (Fig. 8C; for f_R vs. distance plots, in the 0–300 μm range, exponential fit (cf. Fig. 1C): τ=83.3 μm, χ_2 = 3.16; sigmoidal fit (cf. Fig. S2A) $x_{1/2}$ = 239.39 μm; κ = 32.78 μm; χ_2 = 0.735). We also could approximately match the input resistance profile (Fig. 8C) and the *Q* profile (Fig. S13A). We conclude that experimentally observed gradient in density of *h*-channels could theoretically account for experimentally observed gradient in resonance properties.

Global plasticity in I_h is required for global plasticity in resonance and excitability

From our ATBF and ATBP experiments (Figs. 4–5), we know that plasticity in resonance properties and excitability express across a broad region of the apical dendritic tree. However, we do not know if these changes are a result of local or global changes in I_h. To address this question, we employed our multi-compartmental model with I_h distributed as in Fig. 8B. We considered three possible configurations for the expression of plasticity in I_h: (i) plasticity confined to the soma (Fig. 8D, LS); (ii) plasticity confined to a local dendritic segment (Fig. 8D, LD; equal amount of plasticity in 200–300 μm range of the apical trunk); and (iii) plasticity expressed across the entire dendritic tree (Fig. 8D, GL).

To effectuate an increase in I_h, we either increased $\bar{g}_h$ or shifted the activation curve in the depolarizing direction, given that graded increase in f_R can be obtained by either of these manipulations (Fig. 7). Under each of these two cases (increasing $\bar{g}_h$ and depolarizing $V_{1/2}$), we assessed the effects of increasing I_h (on f_R and $\bar{R}_{in}$) as specified by the three possible configurations listed above (LS, LD and GL). Our results indicated that irrespective of whether I_h is increased through an increase in $\bar{g}_h$ or through a depolarizing shift of the activation curve, a global increase in I_h is required to bring about a global increase in resonance properties (Fig.

8F, I; Fig. S13) or a global decrease in R_{in} (Fig. 8G, J). More specifically, the locus of plasticity in both input resistance and f_R reflect the locus of plasticity in I_h. If plasticity in I_h is confined either to the soma or to a local dendritic segment, changes in both these parameters are confined to regions adjacent to the region of expression of I_h plasticity (Fig. 8, Fig. S14). Thus, we conclude that plasticity in I_h has to express across a broad region of the dendritic tree in order to achieve the spatially widespread changes observed in resonance properties and input resistance in our experiments (Fig. 4–5).

DISCUSSION

The primary conclusion of this study is that the intrinsic oscillatory dynamics of a pyramidal neuron are variable and plastic as a consequence of the spatial heterogeneity and plasticity of a voltage-gated ion channel. Specifically, we found that the intrinsic resonance frequency of CA1 neurons varied more than three-fold as a function of dendritic location, due to the spatial gradient in density of *h*-channels. Furthermore, the resonance frequency could be modified by activity-dependent long-term plasticity, which expressed over a broad region of the somato-apical trunk. This increase in resonance frequency, along with an associated reduction in excitability, remained spatially widespread even when they were accompanied by input-specific LTP. Finally, employing computational analyses, we also argued that such spatially widespread changes in resonance frequency and input resistance required changes in *h*-channel properties to span a broad region of the dendritic tree.

Previous studies of plasticity in oscillatory properties of neurons have focused largely on action potential firing patterns of neurons in pacemaker nuclei in electric fish (Oestreich et al., 2006), pre-Botzinger complex (Ramirez et al., 2004) and cultured vertebrate (Guertin and Hounsgaard, 2006) and invertebrate (Haedo and Golowasch, 2006; Harris-Warrick and Marder, 1991; Turrigiano et al., 1994) neurons. Change in intrinsic subthreshold oscillatory dynamics as a function of plasticity in voltage-gated ion-channels has surprisingly remained unexplored, despite the numerous roles that these oscillations play in single neuron and network behavior (Alonso and Garcia-Austt, 1987; Buzsaki, 2002; Hutcheon and Yarom, 2000; Llinas, 1988; Schaefer et al., 2006; Strohmann et al., 1994). Expanding on our results on variability and plasticity in intrinsic resonance, we outline some important implications of these to information processing in the hippocampus.

The pyramidal neuron as a stimulus-dependent matched filter

The impedance amplitude profile is a direct measure of the neuron's response to inputs of various frequencies (Hutcheon and Yarom, 2000; Strohmann et al., 1994). A CA1 pyramidal neuron (Fig. S1C) functions as a band-pass filter that is optimally tuned to respond to frequencies centered on its resonance frequency. We have demonstrated that this center frequency varies as a function of spatial location in the dendrites (Fig. 1C; Fig. S2B). Our results suggest that proximal regions of CA1 pyramidal neurons that receive inputs from area CA3, are tuned to a lower band of frequencies (2–6 Hz), compared to distal regions which receive inputs from the entorhinal cortex (5–10 Hz). Under such a configuration, signals from these two pathways, driven by their differential points of contact on the dendritic arbor, are filtered differently before integration occurs at the soma. Such a design is reminiscent of a matched filter that is designed to match the spectral signature of the corresponding input to maximize the signal-to-noise ratio (Turin, 1960). If a CA1 pyramidal neuron implemented such a design, it would suggest that the inputs from the entorhinal cortex should belong to a higher frequency band than those arriving from the CA3 region. While we do not have direct evidence for this possibility (even though the existence of two independent theta sources is known (Buzsaki, 2002)), this *localized* filtering capability reflecting the spectral signature of various impinging inputs onto a *single* neuron constitutes a novel contribution of dendritic ion channels

to signal integration. Neurons endowed with active dendritic trees can optimally tune their responses to multiple input sources by locally adjusting their active properties (I_h, in this case).

There have been previous studies, prominently in the auditory and the visual systems, where single neurons have been shown to implement such matched filters for maximizing signal-to-noise ratio (Mortensen and Nachtigall, 2000; Ricci et al., 2005). Most of these studies have focused on different neurons tuned either to different frequencies, or to different aspects of the visual stimuli. In contrast, our suggestion pertains to different regions *within a single neuron* tuned to different frequency bands, with local dendritic ion channel properties playing a role in maximizing signal-to-noise ratio across different inputs to the neuron. Further, there have also been theoretical studies linking homeostasis (see below) and matched filters, which suggest that neurons adapting according to a stabilized Hebb rule evolve into a matched filter for the inputs that the neuron receives (Mortensen and Nachtigall, 2000).

There have also been previous studies about another resonance phenomenon associated with filtering along a dendritic cable (transfer impedance) in cortical pyramidal neurons (Ulrich, 2002). Although resonance with respect to the transfer impedance can offer insights into intraneuronal filtering and the role of ion channels in the transfer of information within the neuron (Ulrich, 2002), it would not provide a measure of how the neuron responds locally to external inputs (input impedance) arriving at various dendritic locations. Our study demonstrates that the resonance frequency associated with this input impedance is location-dependent, thus revealing the possibility of a single neuron as a localized, stimulus-dependent matched filter mediated by the density of an ion-channel.

Stimulus-adaptive plasticity in frequency response

A CA1 pyramidal neuron responds to increased activity in two ways: (i) a reduction in input resistance (Fig. 3); and (ii) an increase in its optimal response frequency (Fig. 3C). The former may be considered as a homeostatic mechanism, and is discussed in detail below. We postulate that the latter constitutes a previously unknown ability of a neuron to adapt its frequency response to optimally match the frequency of its inputs. In other words, we suggest that a CA1 pyramidal neuron can act as an adaptive matched filter, capable of tuning its frequency response to optimally and adaptively match the characteristics of inputs it receives. Such adaptability of neuronal responses to statistics of converging network activity has been argued to provide optimality in neural coding (Fairhall et al., 2001;Stemmler and Koch, 1999).

Though the time scale and the level of analysis are different, such adaptation of the system's responses to the environment has been well characterized, especially, in the visual system (Hirsch and Spinelli, 1970; Wiesel and Hubel, 1963). Further, it has also been suggested that the visual system tunes its responses to the spatiotemporal statistics of natural signals, and any alteration to these statistics also leads to an adaptation in the system response (Simoncelli and Olshausen, 2001). The mechanism proposed here can act as a substrate towards achieving similar adaptability in terms of a *single neuron's* response with respect to network activity statistics.

This ability of the neuron also suggests that a single neuron's frequency response properties could be a measure of recent activity of the network it resides in. Further, as in the CA1 pyramidal neuron, subthreshold frequency response seems to be largely guided by the *h*-conductance, this possibility also suggests that the magnitude of the I_h current could act as a measure of recent network activity, with a direct relationship between activity levels and I_h magnitude. This suggestion is consistent with findings that increased network activity, using high potassium external solution, increases the levels of HCN1 protein (Fan et al., 2005).

I_h as a plasticity regulation mechanism

Hebbian synaptic plasticity acts as a positive feedback mechanism, and can destabilize a neuronal network unless concomitant homeostatic processes that can counterbalance this are activated (Turrigiano and Nelson, 2000). It has been argued that such homeostatic processes, to be effective, have to act globally and affect all synapses even if the associated synaptic plasticity is local (Bienenstock et al., 1982; Turrigiano and Nelson, 2000). This requirement on global expression of homeostatic plasticity is particularly true for CA1 pyramidal neurons for two further reasons: (i) input specificity of LTP (Fig. 6), which implicates the involvement of local signals (calcium, for instance) in determining and driving plasticity confined to only certain synapses (Bliss and Collingridge, 1993), rules out a local mechanism to control plasticity across all synapses in the dendritic tree; and (ii) the electrotonic properties of the CA1 pyramidal neuron, which suggest that any local change of conductances does not electrically affect the entire tree (Fig. 8).

We have argued that I_h can act as a potential homeostatic mechanism for regulating plasticity by modulating intracellular calcium entry, indirectly through changes in dendritic excitability (Narayanan et al., Society for Neuroscience abstract, 737.5, 2005). The spatially widespread expression of plasticity in I_h associated with LTP leading to non-local changes in temporal summation (Fig. 5, 6, 8) adds more evidence to this possibility that I_h could act as a mechanism driving metaplasticity in hippocampal synapses.

In conclusion, employing resonance as a tool, we have demonstrated that a single pyramidal neuron can display different oscillatory dynamics at different points of its dendritic tree, and that its oscillatory dynamics can be modulated by activity, as consequences of changes in a voltage-gated ion channel. Given that select voltage-gated ion channels mediate intrinsic oscillatory dynamics (Hu et al., 2002; Hutcheon and Yarom, 2000; Llinas, 1988), and that activity-dependent modulation of such ion channels is well established (Cantrell and Catterall, 2001; Delmas and Brown, 2005; Robinson and Siegelbaum, 2003), potential implications of our findings are not confined to the hippocampus, but extend to other brain regions with neurons exhibiting intrinsic oscillations. Importantly, owing to the numerous roles that intrinsic oscillations are known to play, studies probing intrinsic plasticity of oscillatory dynamics can offer valuable insights into information processing in single neurons and their networks. Specifically, future studies could focus on physiological implications of such plasticity to frequency selectivity (Hutcheon and Yarom, 2000; Strohmann et al., 1994), stimulus-adaptability of neuronal responses (Fairhall et al., 2001; Stemmler and Koch, 1999), homeostasis (Mortensen and Nachtigall, 2000; Turrigiano and Nelson, 2000), spike precision (Schaefer et al., 2006), generation of network rhythms and synchrony (Alonso and Garcia-Austt, 1987; Bland and Colom, 1993; Buzsaki, 2002), apart from the relevance of these to various behavioral states (Buzsaki, 2002; O'Keefe and Burgess, 2005).

EXPERIMENTAL PROCEDURES

Electrophysiology

Near-horizontal 350 μm hippocampal slices were prepared from 5–7 weeks old male Sprague Dawley rats using standard procedures (Fan et al., 2005). The standard extracellular recording solution contained (in mM) 125 NaCl, 3 KCl, 1.25 NaH_2PO_4, 25 $NaHCO_3$, 2 $CaCl_2$, 1 $MgCl_2$ and 10 dextrose. Slices were incubated, for at least an hour, in a similar solution, but contained 2.5 mM KCl and 2 mM $MgCl_2$, in addition to 3 mM sodium pyruvate and 1.3 mM ascorbic acid. Characterization experiments (Figs. 1–2) were carried out with 10 μM CNQX, 10 μM (+)bicuculline, 10 μM picrotoxin, 50 μM D, L-APV and 2 μM CGP55845 added to the standard solution. While TBF experiments (Fig. 3) were performed with the standard external solution, for ATBF experiments (Fig. 4), 10 μM CNQX, 10 μM (+)bicuculline, 10 μM

picrotoxin and 2 μM CGP55845 were added to the standard solution. ATBP (Fig. 5–6) and TBP (Fig. 6) experiments were performed with 10 μM (+)bicuculline, 10 μM picrotoxin and 2 μM CGP55845 in the standard solution. Whenever GABA receptors were blocked, area CA3 was removed to diminish repetitive firing. The whole-cell recording pipette solution contained (in mM) 120 K-gluconate, 20 KCl, 10 HEPES, 2 NaCl, 4 MgATP, 0.3 tris-GTP, 7 tris-phosphocreatine (pH 7.3). Neurons were visualized with differential interference contrast microscopy using a Zeiss Axioskop microscope, fitted with a 60X (Olympus) water-immersion objective. Whole-cell patch recordings in current-clamp mode were made from the soma or the dendrites of CA1 pyramidal neurons using a Dagan IX2-700 amplifier. Signals were filtered at 5 kHz and sampled at 10–50 kHz. Recordings were made at 33–35° C. Electrodes were pulled from borosilicate glass, and their resistance was 4–6 MΩ for somatic recordings and 5–7 MΩ for dendritic recordings. During the course of the experiments, an estimate of the neuron's input resistance (denoted by $\bar{R}_{in}$) was measured from the steady state response of the cell to a 100 pA hyperpolarizing current pulse, which also was used to monitor and compensate, if necessary, for changes in series resistance. Access resistance was 10–25 MΩ for somatic recordings, and 20–40 MΩ for dendritic recordings through the period of the experiment. Data acquisition and analysis were performed with custom-written software in the *Igor Pro* environment (Wavemetrics).

Measurements

Input resistance (R_{in}) was measured as the slope of a linear fit to the steady state V-I plot obtained by injecting subthreshold current pulses of amplitudes spanning −50 pA to 50 pA, in steps of 10 pA (note that this is different from $\bar{R}_{in}$, above). Action potential firing frequency was computed by extrapolating the number of spikes obtained during a 700 ms current injection to 1 s. Stimulus used for characterizing the impedance amplitude profile (ZAP) was a sinusoidal current of constant amplitude, with its frequency linearly spanning 0–20 Hz in 20 s (ZAP20; Fig. S1 A). The ZAP stimulus used for plasticity experiments (Figs. 3–6) had its frequency linearly span 0–15 Hz in 15 s (ZAP 15; Fig. S5B). The reason behind using a shorter version of the ZAP stimulus was to obtain two responses to the stimulus per minute, with enough inter-stimulus interval to compensate for series resistance changes, if necessary. The magnitude of the ratio of the Fourier transform of the voltage response to the Fourier transform of the ZAP stimulus formed the impedance amplitude profile. The frequency at which the impedance amplitude reached its maximum was the resonance frequency (f_R). Resonance strength (Q) was measured as the ratio of the maximum impedance amplitude to the impedance amplitude at 0.5 Hz (Hu et al., 2002). Percentage sag was measured from the voltage response of the cell to a hyperpolarizing current pulse of 100 pA, and was defined as $100*(1 - V_{ss}/V_{peak})$, where V_{ss} was the steady-state voltage deflection from baseline and V_{peak} was the peak voltage deflection from baseline. EPSP slope was computed as the slope of the linear fit to the initial 2 ms rising period of an EPSP. α-EPSPs were evoked by α current injections of the form $I_\alpha = I_{max}\, t \exp(-\alpha\, t)$, with $\alpha = 0.1$. Temporal summation ratio in a train of EPSPs was computed as E_{last}/E_{first}, where E_{last} and E_{first} were the amplitudes of last and first EPSPs in the train respectively. Voltages have not been corrected for the theoretical liquid junction potential, which was calculated to be ~ 14 mV based on relative ionic mobilities and charge.

Plasticity protocols

The experimental protocol for TBF (Fig. 3) and ATBF (Fig. 4) experiments involved an establishment of a five-minute stable baseline of f_R and $\bar{R}_{in}$ (both measured from the ZAP15 stimulus), following an initial measurement of *V–I* (voltage vs. current plot to measure R_{in}) *and f–I* (action potential frequency as a function of depolarizing current injections) curves. Responses to the ZAP15 stimulus were measured, twice every minute, for 40 minutes after induction of plasticity, followed by a final measurement of the *V–I* and *f–I* curves. In addition to these, in ATBP (Fig. 5–6) and TBP (Fig. 6) experiments, stable baselines of evoked EPSPs

were established (3–5 mV peak), and were monitored after plasticity induction with measurements made twice every minute. In two-pathway TBP experiments (Fig. 6), evoked EPSPs from both pathways were measured twice every minute, with the measurement of the two EPSPs separated by ~ 16 seconds (on either side of the ZAP15 stimulus). Details of plasticity induction for each of these cases are provided in respective figure legends. For all plasticity experiments, recordings were carried out at the initial resting membrane potential through the course of the experiment.

Data analysis

In characterization experiments (Figs. 1–2), values at each "holding voltage" were averages of measurements obtained by injecting the ZAP20 stimulus five times. In plasticity experiments (Figs. 3–6), baseline values of EPSP slope, f_R, sag and Q were obtained by averaging measurements over the entire five minute baseline period, and post-plasticity values were obtained by averaging measurements from the 35–40 minute period after induction of plasticity. For time course plots *(e.g.* Fig. 3E), two successive measurements were averaged to obtain a single data value for each minute, and this value was divided by the average baseline value throughout to obtain the normalized time course. Group data are expressed as mean ± SEM. Depending on the dataset, statistical significance was calculated using paired or unpaired *Student's t* tests, *Mann-Whitney, ANOVA,* or the *Kruskal-Wallis* tests. Post hoc tests following significance with the *Kruskal-Wallis* test were performed with the *Dunn's* test. Correlation was assessed using the *Pearson's* correlation test.

Computer simulations

Simulations were performed using the NEURON simulation environment (Carnevale and Hines, 2006). Integration time step for all simulations was set at 25 μs. Temperature was set at 34° C. The single compartment model (Fig. S11A) was a cylinder of 100 μm length and 100 μm diameter. R_m was set as 30 kΩ-cm^2, and C_m was 1 μF/cm^2. ZAP20 current stimulus (Fig. S1A) was injected to obtain measurements of f_R and $\bar{R}_{in}$ under various parametric variations. The kinetics of the only active mechanism in the model, the *h*-channel, were set in accordance with experimental measurements (Fig. S11B) from the CA1 pyramidal neuron (Magee, 1998). Cell *n123* (Fig. 8A) from the Duke-Southampton archive (http://neuron.duke.edu/cells/) was used for all multicompartmental simulations. Passive properties were set as in (Poirazi et al., 2003). All multicompartmental simulations were performed at −65 mV.

Supplementary Material

Refer to Web version on PubMed Central for supplementary material.

Acknowledgements

The authors thank Drs. Xixi Chen, Raymond Chitwood, Richard Gray, Amiel Rosenkranz, Clifton Rumsey and Mr. Yul Young Park for providing help through various phases of this study. They also thank Dr. Richard Gray for writing the data acquisition software and all members of the laboratory for comments on the draft manuscript. The International Human Frontier Science Program Organization (RN) and the National Institutes of Health (Grants to DJ: MH48432, MH44754, NS37444) supported this study.

References

Alonso A, Garcia-Austt E. Neuronal sources of theta rhythm in the entorhinal cortex of the rat. II. Phase relations between unit discharges and theta field potentials. Exp Brain Res 1987;67:502–509. [PubMed: 3653312]

Bienenstock EL, Cooper LN, Munro PW. Theory for the development of neuron selectivity: orientation specificity and binocular interaction in visual cortex. J Neurosci 1982;2:32–48. [PubMed: 7054394]

Bland BH, Colom LV. Extrinsic and intrinsic properties underlying oscillation and synchrony in limbic cortex. Prog Neurobiol 1993;41:157–208. [PubMed: 8332751]

Bliss TV, Collingridge GL. A synaptic model of memory: long-term potentiation in the hippocampus. Nature 1993;361:31–39. [PubMed: 8421494]

Buzsaki G. Theta oscillations in the hippocampus. Neuron 2002;33:325–340. [PubMed: 11832222]

Cantrell AR, Catterall WA. Neuromodulation of Na+ channels: an unexpected form of cellular plasticity. Nat Rev Neurosci 2001;2:397–407. [PubMed: 11389473]

Carnevale, NT.; Hines, ML. The NEURON Book. Cambridge University Press; 2006.

Delmas P, Brown DA. Pathways modulating neural KCNQ/M (Kv7) potassium channels. Nat Rev Neurosci 2005;6:850–862. [PubMed: 16261179]

Engel AK, Fries P, Singer W. Dynamic predictions: oscillations and synchrony in top-down processing. Nat Rev Neurosci 2001;2:704–716. [PubMed: 11584308]

Fairhall AL, Lewen GD, Bialek W, de Ruyter Van Steveninck RR. Efficiency and ambiguity in an adaptive neural code. Nature 2001;412:787–792. [PubMed: 11518957]

Fan Y, Fricker D, Brager DH, Chen X, Lu HC, Chitwood RA, Johnston D. Activity-dependent decrease of excitability in rat hippocampal neurons through increases in I(h). Nat Neurosci 2005;8:1542–1551. [PubMed: 16234810]

Frick A, Magee J, Johnston D. LTP is accompanied by an enhanced local excitability of pyramidal neuron dendrites. Nat Neurosci 2004;7:126–135. [PubMed: 14730307]

Guertin PA, Hounsgaard J. Conditional intrinsic voltage oscillations in mature vertebrate neurons undergo specific changes in culture. J Neurophysiol 2006;95:2024–2027. [PubMed: 16236781]

Haedo RJ, Golowasch J. Ionic mechanism underlying recovery of rhythmic activity in adult isolated neurons. J Neurophysiol 2006;96:1860–1876. [PubMed: 16807346]

Harris-Warrick RM, Marder E. Modulation of neural networks for behavior. Annu Rev Neurosci 1991;14:39–57. [PubMed: 2031576]

Hirsch HV, Spinelli DN. Visual experience modifies distribution of horizontally and vertically oriented receptive fields in cats. Science 1970;168:869–871. [PubMed: 5444065]

Hu H, Vervaeke K, Storm JF. Two forms of electrical resonance at theta frequencies, generated by M-current, h-current and persistent Na+ current in rat hippocampal pyramidal cells. J Physiol 2002;545:783–805. [PubMed: 12482886]

Hutcheon B, Miura RM, Puil E. Models of subthreshold membrane resonance in neocortical neurons. J Neurophysiol 1996;76:698–714. [PubMed: 8871192]

Hutcheon B, Yarom Y. Resonance, oscillation and the intrinsic frequency preferences of neurons. Trends Neurosci 2000;23:216–222. [PubMed: 10782127]

Leung LS, Yu HW. Theta-frequency resonance in hippocampal CA1 neurons in vitro demonstrated by sinusoidal current injection. J Neurophysiol 1998;79:1592–1596. [PubMed: 9497437]

Leung LW, Yim CY. Intrinsic membrane potential oscillations in hippocampal neurons in vitro. Brain Res 1991;553:261–274. [PubMed: 1718544]

Llinas RR. The intrinsic electrophysiological properties of mammalian neurons: insights into central nervous system function. Science 1988;242:1654–1664. [PubMed: 3059497]

Lorincz A, Notomi T, Tamas G, Shigemoto R, Nusser Z. Polarized and compartment-dependent distribution of HCN1 in pyramidal cell dendrites. Nat Neurosci 2002;5:1185–1193. [PubMed: 12389030]

Magee JC. Dendritic hyperpolarization-activated currents modify the integrative properties of hippocampal CA1 pyramidal neurons. J Neurosci 1998;18:7613–7624. [PubMed: 9742133]

Marder E, Calabrese RL. Principles of rhythmic motor pattern generation. Physiol Rev 1996;76:687–717. [PubMed: 8757786]

Mortensen U, Nachtigall C. Visual channels, Hebbian assemblies and the effect of Hebb's rule. Biol Cybern 2000;82:401–413. [PubMed: 10836586]

O'Keefe J, Burgess N. Dual phase and rate coding in hippocampal place cells: theoretical significance and relationship to entorhinal grid cells. Hippocampus 2005;15:853–866. [PubMed: 16145693]

Oestreich J, Dembrow NC, George AA, Zakon HH. A "sample-andhold" pulse-counting integrator as a mechanism for graded memory underlying sensorimotor adaptation. Neuron 2006;49:577–588. [PubMed: 16476666]

Poirazi P, Brannon T, Mel BW. Arithmetic of subthreshold synaptic summation in a model CA1 pyramidal cell. Neuron 2003;37:977–987. [PubMed: 12670426]

Ramirez JM, Tryba AK, Pena F. Pacemaker neurons and neuronal networks: an integrative view. Curr Opin Neurobiol 2004;14:665–674. [PubMed: 15582367]

Ricci AJ, Kennedy HJ, Crawford AC, Fettiplace R. The transduction channel filter in auditory hair cells. J Neurosci 2005;25:7831–7839. [PubMed: 16120785]

Robinson RB, Siegelbaum SA. Hyperpolarization-activated cation currents: from molecules to physiological function. Annu Rev Physiol 2003;65:453–480. [PubMed: 12471170]

Schaefer AT, Angelo K, Spors H, Margrie TW. Neuronal oscillations enhance stimulus discrimination by ensuring action potential precision. PLoS Biol 2006;4:e163. [PubMed: 16689623]

Simoncelli EP, Olshausen BA. Natural image statistics and neural representation. Annu Rev Neurosci 2001;24:1193–1216. [PubMed: 11520932]

Stemmler M, Koch C. How voltage-dependent conductances can adapt to maximize the information encoded by neuronal firing rate. Nat Neurosci 1999;2:521–527. [PubMed: 10448216]

Steriade M, Timofeev I. Neuronal plasticity in thalamocortical networks during sleep and waking oscillations. Neuron 2003;37:563–576. [PubMed: 12597855]

Strohmann B, Schwarz DW, Puil E. Subthreshold frequency selectivity in avian auditory thalamus. J Neurophysiol 1994;71:1361–1372. [PubMed: 8035220]

Turin GL. An introduction to matched filters. IRE transactions on information theory 1960;6:311–329.

Turrigiano G, Abbott LF, Marder E. Activity-dependent changes in the intrinsic properties of cultured neurons. Science 1994;264:974–977. [PubMed: 8178157]

Turrigiano GG, Nelson SB. Hebb and homeostasis in neuronal plasticity. Curr Opin Neurobiol 2000;10:358–364. [PubMed: 10851171]

Ulrich D. Dendritic resonance in rat neocortical pyramidal cells. J Neurophysiol 2002;87:2753–2759. [PubMed: 12037177]

Volgushev M, Chistiakova M, Singer W. Modification of discharge patterns of neocortical neurons by induced oscillations of the membrane potential. Neuroscience 1998;83:15–25. [PubMed: 9466396]

Wiesel TN, Hubel DH. Single-Cell Responses In Striate Cortex Of Kittens Deprived Of Vision In One Eye. J Neurophysiol 1963;26:1003–1017. [PubMed: 14084161]

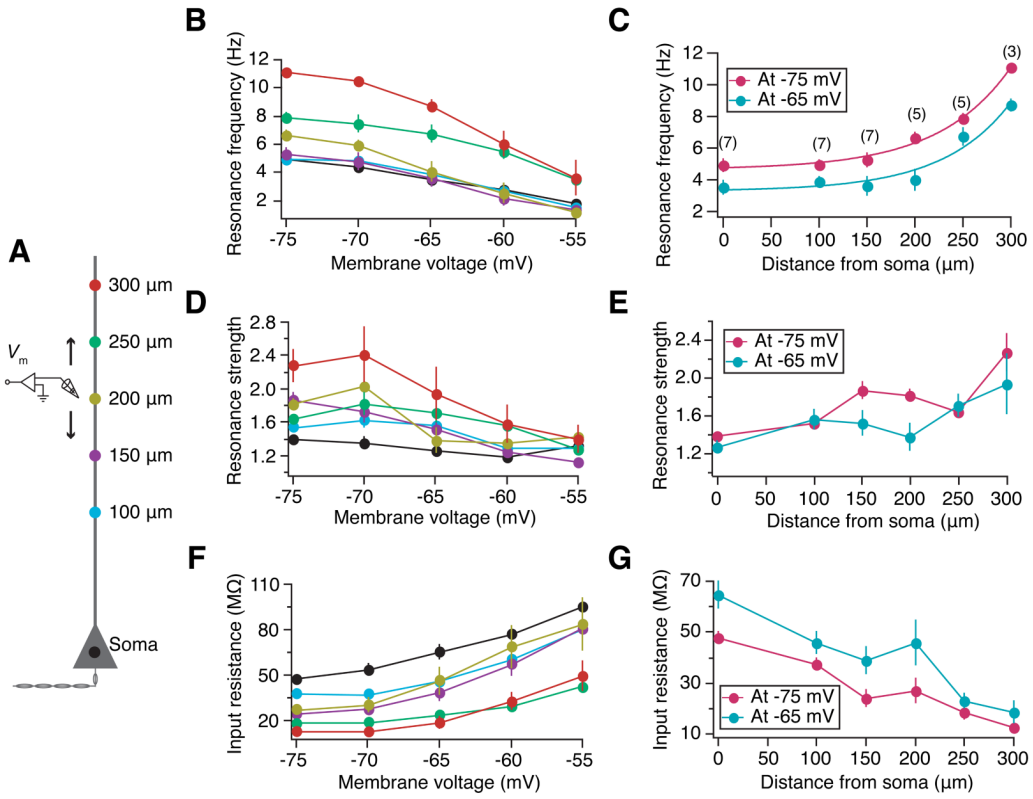

Figure 1.

Resonance frequency in dendrites increases exponentially with distance from the soma. (A) Schematic of the somato-apical trunk, depicting the experimental design for assessing the resonance properties as a function of distance from the soma. Voltage responses of the soma and dendrites at various distances (up to 320 µm away from the soma) to the ZAP20 stimulus (Fig. S1A) were recorded locally using a whole-cell patch-clamp electrode (V_m). Colors of markers along the somato-apical trunk serve as codes for corresponding distances in (B), (D) and (F). (B) In the subthreshold voltage range, irrespective of distance from soma, resonance frequency increases with membrane hyperpolarization. (C) Dendritic resonance frequency increases exponentially (Exponential fit: **−75 mV**: τ = 74.38 µm; **−65 mV:** τ = 70.18 µm) with distance from the soma. Markers (●: measured at −75 mV; ●: measured at −65 mV) correspond to experimental values, and solid lines indicate exponential fits to respective experimental values. The number within parenthesis at each distance value is the number of somatic or dendritic recordings performed to arrive at the population plots in (B–G). Irrespective of distance from soma, resonance strength increases (D), and input resistance ($\bar{R}_{in}$) decreases (F) with membrane hyperpolarization. Resonance strength increases (E) and $\bar{R}_{in}$ decreases (G) with increase in distance from soma.

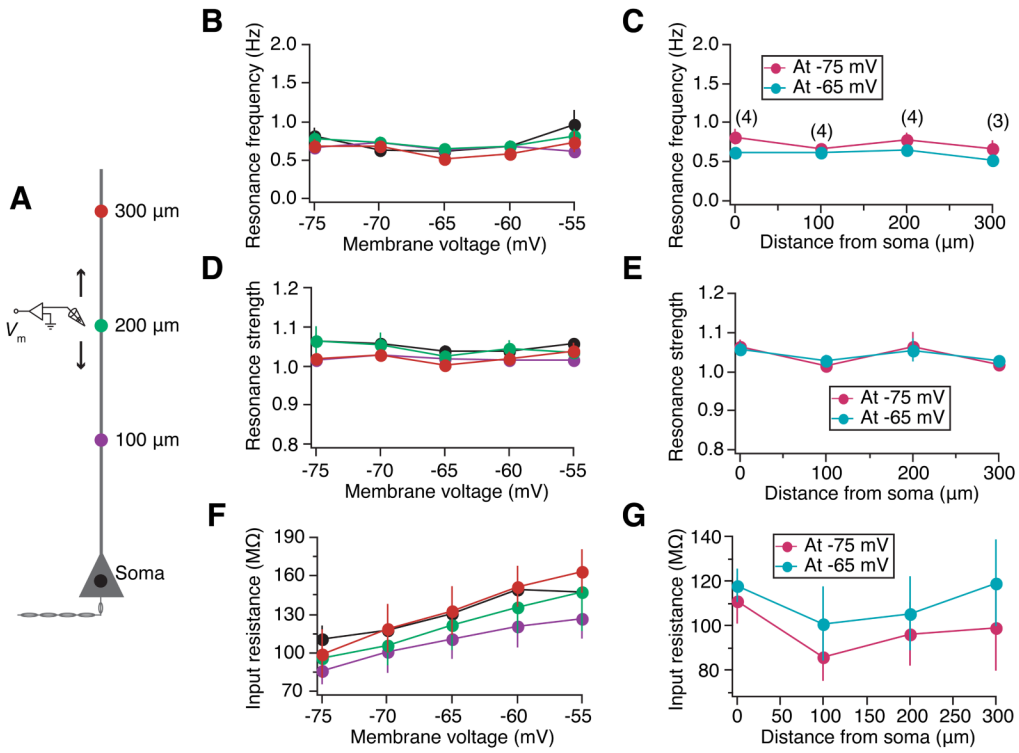

Figure 2.

Pretreatment with ZD7288 abolishes subthreshold resonance across the dendritic tree. (A) Schematic of the somato-apical trunk, with colors of markers along the somato-apical trunk serving as codes for corresponding distances in (B), (D) and (F). Plots in (B–G) were derived from somatic or dendritic recordings obtained from slices pretreated (for 5 minutes) with ZD7288 (100 µM). At all subthreshold voltages, and at all distances from the soma, resonance frequency reduces to less than 1 Hz (B) and (C), and resonance strength is closer to 1 (D) and (E). (F) Irrespective of distance from soma, input resistance ($\bar{R}_{in}$) decreases with membrane hyperpolarization. (G) $\bar{R}_{in}$ does not change significantly with distance from the soma.

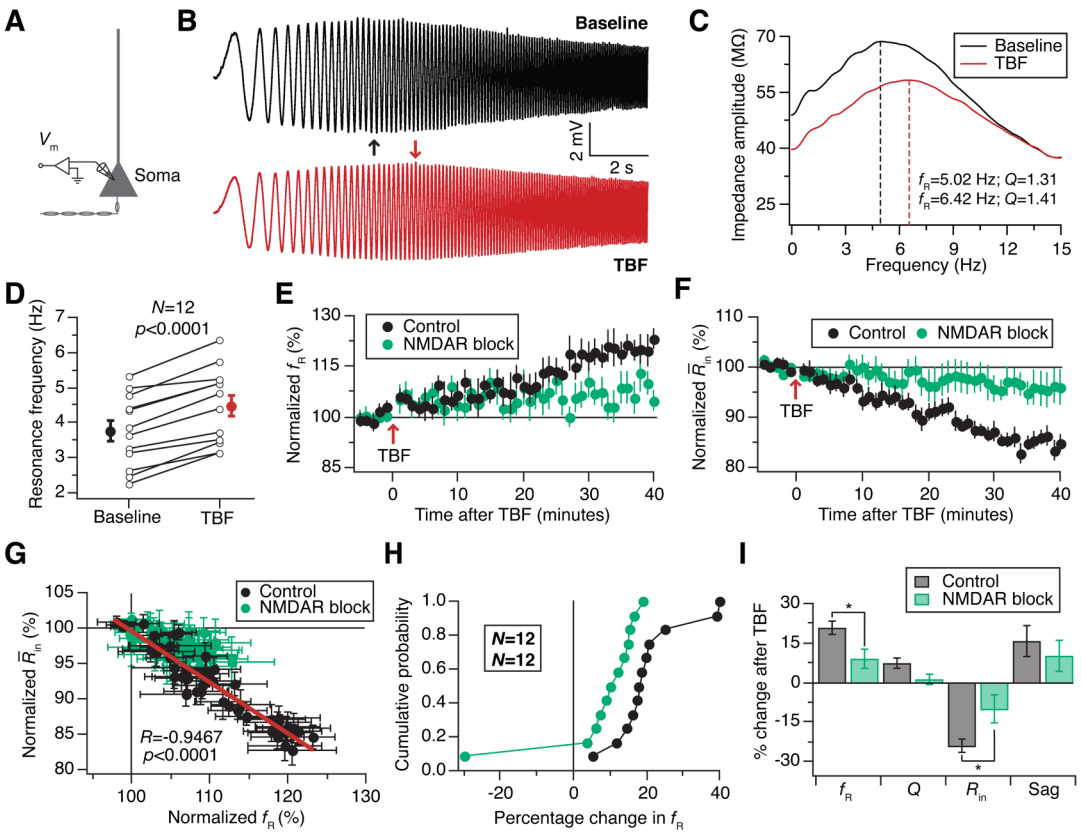

Figure 3.

Theta burst firing (TBF) elicits an NMDAR-dependent increase in resonance frequency (f_R). (A) Schematic of the somato-apical trunk depicting the experimental design for assessing plasticity in excitability and resonance properties of the soma. Voltage responses of the soma were recorded using a whole-cell patch-clamp electrode (V_m). Induction of plasticity was carried out by theta burst firing through somatic current injections (Fig. S5C). (B) Response of the neuron to the ZAP 15 stimulus (Fig. S5B) during the baseline period and 40 minutes after TBF. Arrows in corresponding colors indicate the location of maximal response in each trace, indicating a rightward shift in this location in the TBF trace with respect to that in the baseline trace. (C) Impedance amplitude as a function of frequency computed from correspondingly color-coded traces in (B). 40 minutes after TBF, there is an increase in f_R and resonance strength (Q) with respect to baseline. (D) Population data of f_R measured before (●) and 40 minutes after TBF (●) shows a significant increase (paired *Student's t*-test, Baseline: 3.75 ± 0.3 Hz; TBF: 4.57 ± 0.31 Hz) after TBF. (E)–(I) NMDAR antagonists (50 μM D, L-APV and 10 μM (+)MK801) suppress TBF-induced plasticity in f_R and $\bar{R}_{in}$. Time courses of normalized f_R (E) and $\bar{R}_{in}$ (F) during TBF experiments (●) are compared to those during TBF experiments in the presence of NMDAR antagonists (●). (G) Relationship between TBF-induced changes in f_R and $\bar{R}_{in}$ in control experiments (●) and in experiments with NMDAR antagonists (●). The red line shows a linear fit to the control points, and the R and p values correspond to the outcome of the *Pearson's* correlation test on the control points (●). (H) Cumulative probability plot of data in (E). Each point represents the magnitude of change, at 40 minutes after TBF, relative to respective baseline in control (●) or NMDAR block (●) experiments. (I) Summary plot of percentage change in various parameters, at 40 minutes after TBF, relative to respective baseline values in control and NMDAR block experiments. *: $p<0.05$, *Mann-Whitney* test across the two populations. All four parameters were significantly

different ($p<0.05$, paired *Student's t* test) with respect to their baseline values within the Control population, while none of them were significantly different within the NMDAR block population (Fig. S5).

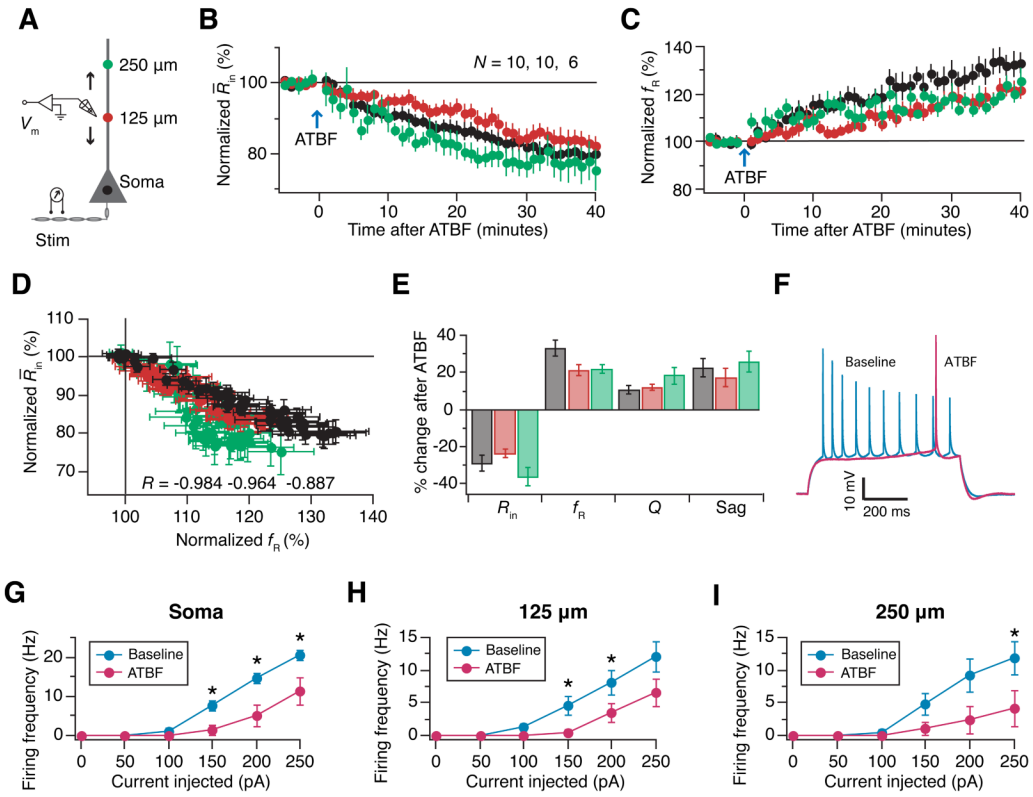

Figure 4.

Antidromic theta burst firing (ATBF) results in a reduction in excitability and an increase in resonance frequency (f_R) across the somato-apical trunk. (A) Schematic of the somato-apical trunk depicting the experimental design for assessing plasticity in excitability and resonance properties as functions of distance from the soma. Voltage responses of the soma and dendrites at various distances (up to around 300 µm from the soma) were recorded locally using a whole-cell patch-clamp electrode (V_m). Induction of plasticity is carried out by theta burst firing elicited by antidromic stimulation (Fig. S6B) through a bipolar tungsten electrode placed in the Alveus. Recordings along the somato-apical trunk are binned into three subpopulations (Soma, 125 µm, and 250 µm) depending on the distance of the recording location from the soma. Colors of markers along the somato-apical trunk serve as codes for corresponding distances in (B–E). Time courses of reduction in $\bar{R}_{in}$ (B) and increase in f_R (C) during ATBF experiments are almost identical for all three locations. (D) Relationship between changes in f_R and $\bar{R}_{in}$ during ATBF experiments at various locations. The color-coded *R* values are the outcomes of the *Pearson's* correlation test on the corresponding populations ($p<0.0001$ for all three cases). (E) Summary plot of percentage change in various parameters, at 40 minutes after ATBF, relative to respective baseline values at various distances from the soma. None of these four measured parameters had significantly different plasticity across the three populations (*Kruskal-Wallis* test, $p>0.05$), implying that ATBF-induced plasticity in all measured parameters is nearly identical across the dendritic tree. All four parameters were significantly different ($p<0.05$, paired *Student's t* test) with respect to their baseline values within all three populations (Fig. S6). (F)-(I) Across the dendritic tree, ATBF results in a significant reduction in action potential firing frequency. (F) Example voltage traces recorded by injecting 200 pA depolarizing current locally to a dendrite 240 µm away from soma before and 40 minutes after ATBF bring out a significant reduction in the number of action potentials fired after ATBF. Population plots of firing frequency as a function of injected current to the soma (G), dendrites

located around 125 μm (H) and 250 μm (I) show significant reductions after ATBF (Baseline:●; 40 min after ATBF: ●) across the dendritic tree. *: $p<0.05$, paired *Student's t* test.

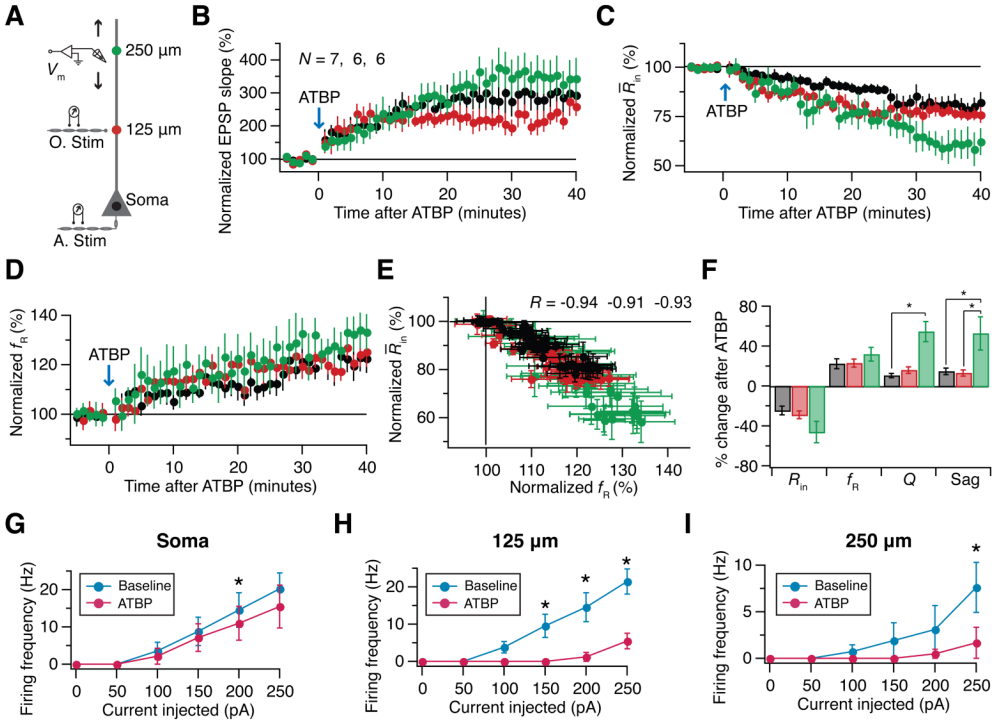

Figure 5.

LTP is accompanied by a reduction in excitability and an increase in resonance frequency (f_R) across the somato-apical trunk. (A) Schematic of the somato-apical trunk depicting the experimental design for assessing LTP-associated plasticity in excitability and resonance properties as functions of distance from the soma. Voltage responses of the soma and dendrites at various distances (up to around 300 µm from the soma) were recorded locally using a whole-cell patch-clamp electrode (V_m). EPSPs were elicited by stimulating the orthodromic pathway (O. Stim) located at around 125 µm from the soma, irrespective of location of the recording electrode. Induction of plasticity (antidromic theta burst pairing; ATBP) is carried out by theta burst pairing (Fig. S7) of orthodromic stimulation (O. Stim) and antidromic stimulation (A. Stim). Recordings along the somato-apical trunk are binned into three subpopulations (Soma, 125 µm, and 250 µm) depending on the distance of the recording location from the soma. Colors of markers along the somato-apical trunk serve as codes for corresponding distances in (B-F). Time courses of increase in EPSP slope (B), reduction in $\bar{R}_{in}$ (C) and increase in f_R (D) during ATBP experiments are almost identical for all three locations (Fig. S8). (E) Relationship between changes in f_R and $\bar{R}_{in}$ during ATBP experiments at various locations. The color-coded *R* values are the outcomes of the *Pearson's* correlation test on the corresponding populations ($p<0.0001$ for all three cases). (F) Summary plot of percentage change in various parameters, at 40 minutes after ATBP, relative to respective baseline values at various distances from the soma. Neither f_R nor $\bar{R}_{in}$ had significantly different plasticity across the three populations (*Kruskal-Wallis* test, $p>0.05$). *: $p<0.05$, *Dunn's* post hoc test following significance with *Kruskal-Wallis* test. All four parameters were significantly different ($p<0.05$, paired *Student's t* test) with respect to their baseline values within all three populations (Fig. S8). (G)-(I) Across the dendritic tree, ATBP results in a significant reduction in action potential firing frequency. Population plots of firing frequency as a function of injected current to the soma (G), dendrites located around 125 µm (H) and 250 µm (I) show significant reductions after ATBP (Baseline:●; 40 min after ATBF: ●) across the dendritic tree. *: $p<0.05$, paired *Student's t* test.

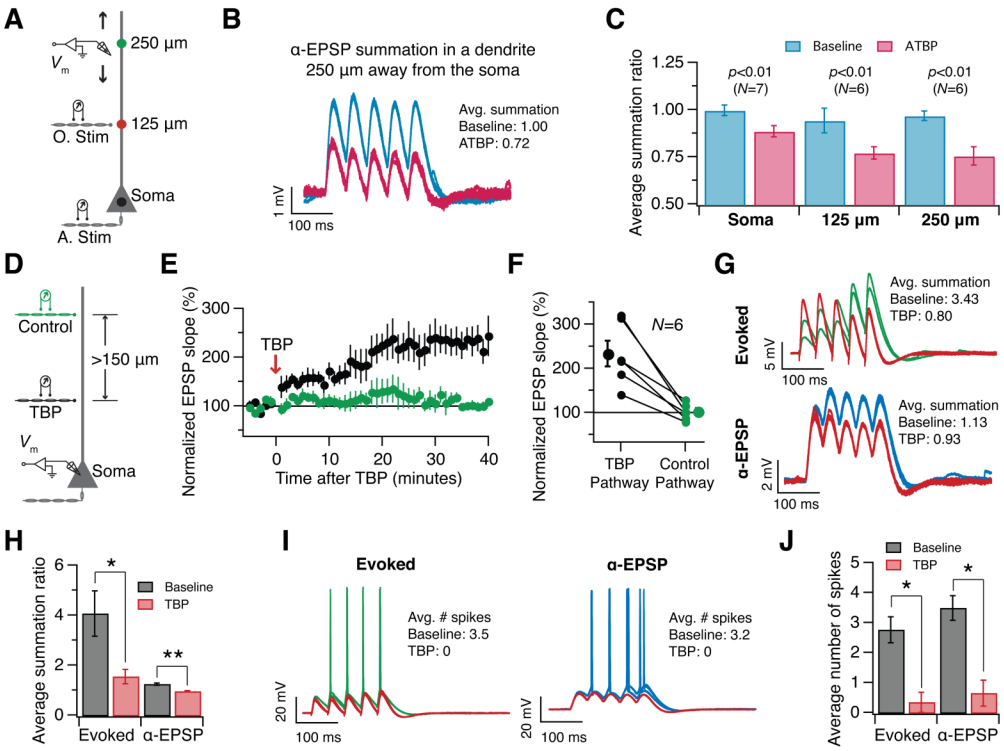

Figure 6.

LTP is accompanied by a non-local reduction in temporal summation. (A)-(C) Antidromic theta burst pairing (ATBP) is accompanied by a reduction in temporal summation of α-EPSPs across the dendritic tree. (A) Schematic of the somato-apical trunk depicting the experimental design for assessing LTP-associated plasticity in temporal summation as a function of distance from the soma. Details are similar to Fig. 5A. (B) Multiple runs of dendritic responses showing a train of 5 α-EPSPs at 20 Hz before and after ATBP. The amplitude of current injection was the same before and after ATBP. ATBP-induced reduction in temporal summation may be observed by comparing the amplitudes of first and last EPSPs in the train. (C) Population plot of average summation ratio before and 40 minutes after ATBP illustrate a significant reduction (paired *Student's t* test) in temporal summation following ATBP across all three populations. (D)-(J) Theta burst pairing (TBP) is accompanied by a non-local reduction in temporal summation of evoked EPSPs. (D) Schematic of the somato-apical trunk depicting the experimental design for assessing LTP-associated plasticity in evoked temporal summation. Voltage responses of the soma were recorded using a whole-cell patch-clamp electrode (V_m). EPSPs were elicited by stimulating either the Control pathway or the TBP pathway. The TBP pathway is located at 115 ± 4.28 µm from the soma, and the Control stimulating electrode is at 283 ± 3.33 µm from the soma. Plasticity is induced by pairing the TBP pathway with postsynaptic action potentials (Fig. S9). Evoked temporal summation is assessed on the Control pathway. (E) TBP leads to pathway-specific LTP. Normalized EPSP slopes during TBP experiments show significant potentiation on the TBP pathway (●), and not on the Control pathway (●). (F) Plot showing difference in potentiation on the TBP (●) against the control (●) pathway for each experiment (35–40 minutes after TBP). (G) Multiple runs of somatic responses showing a train of 5 evoked EPSPs (top) or α-EPSPs (bottom) at 25 Hz before and after TBP. The stimulus intensity (for evoked EPSPs) and the amplitude of current injection (for α-EPSPs) were the same before and after TBP. For both the cases, TBP-induced reduction in temporal summation may be observed by comparing the amplitudes of first and last EPSPs in the train. (H) Population plots of average summation ratio of both evoked EPSPs and α-

EPSPs before and 40 minutes after TBP illustrate a significant reduction (paired *Student's t* test) in temporal summation following TBP. (I) Multiple runs of somatic spike responses showing a train of 5 evoked EPSPs (left) or α-EPSPs (right) at 25 Hz, before and after TBP. These example traces were obtained from the same cell as those shown in (G). The stimulus amplitude (for evoked EPSPs) and amplitude of current injection (for α-EPSPs) were higher than those shown in (G) in order to be able to induce spikes, and were the same before and after TBP. A clear reduction in number of spikes in both the cases may be noted following TBP. (J) Population plot of average number of summation-induced spikes before and 40 minutes after TBP illustrate a significant reduction (paired *Student's t* test) following TBP, for both evoked and α-EPSPs. TBP also induces an increase in resonance frequency and a reduction in excitability (Fig. S9). TBF can also lead to reduction in spikes induced through temporal summation of α-EPSPs (Fig. S10). *:$p<0.05$; **;$p<0.001$.

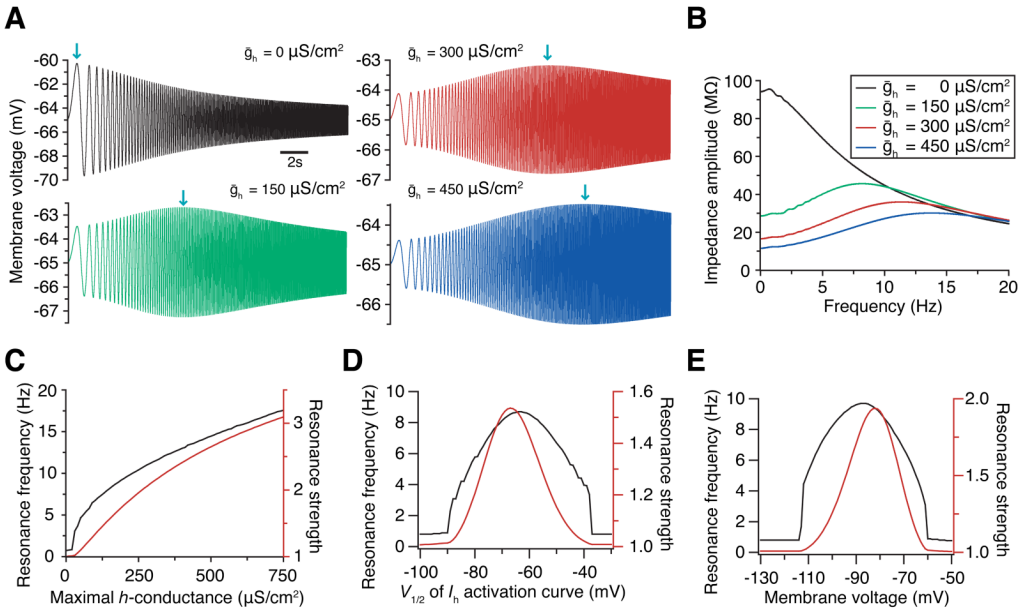

Figure 7.

Simulations reveal a direct relationship between subthreshold resonance and *h*-channel properties. (A) Responses of the single compartment model to the ZAP20 stimulus (Fig. S1A) for various values of the maximal *h*-conductance, $\bar{g}_h$. Arrows indicate the location of maximal response in each trace. A rightward shift in this maximal response location is observed with increase in $\bar{g}_h$. (B) Impedance amplitude profiles of traces in (A), with corresponding color codes, depicting the absence of resonance in the absence of *h*-conductance ($\bar{g}_h$ = 0 μS/cm^2; black) and the increase in resonance frequency (f_R) with increase in $\bar{g}_h$. (C) Systematically varying $\bar{g}_h$ and obtaining f_R and resonance strength (Q) for each value of $\bar{g}_h$ establishes f_R and Q as monotonically increasing functions of $\bar{g}_h$. Performing similar analyses on the $V_{1/2}$ of the I_h activation curve (D) and membrane voltage (E) reveal a bell-shaped dependence of both f_R and Q on both parameters. See Fig. S11 for other parametric dependencies.

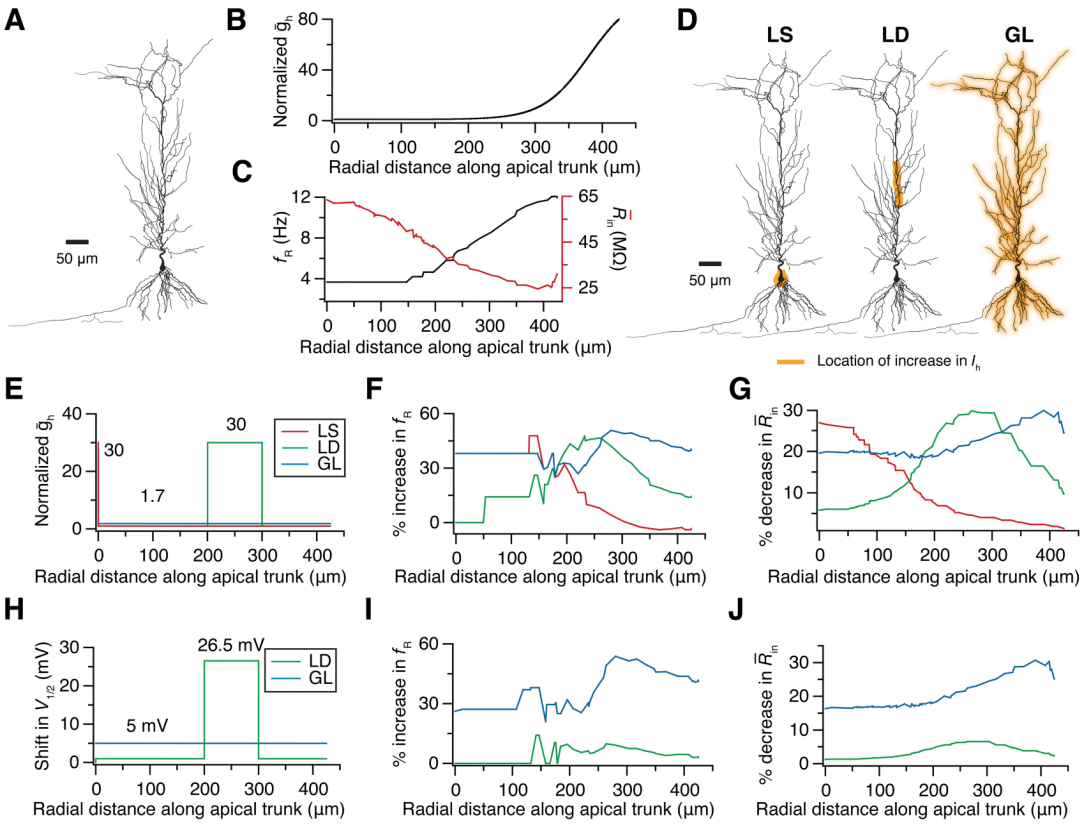

Figure 8.

Multicompartmental simulations indicate that plasticity in I_h has to express globally to elicit global changes in resonance frequency (f_R) and input resistance ($\bar{R}_{in}$). (A) Projection of the three-dimensional neuronal reconstruction used for multicompartment simulations. (B) Profile of $\bar{g}_h$ as a function of radial distance from the soma required to match experimental results (Fig. 1) on f_R and $\bar{R}_{in}$. (C) Profiles of local f_R and local $\bar{R}_{in}$ along the somato-apical trunk as a function of radial distance from the soma in the model cell. (D)–(J) Global changes in I_h are required to elicit global changes in f_R and $\bar{R}_{in}$. (D) Graphical illustration of the three different possibilities tested with simulations on the location of increase in I_h. Left: expression of plasticity is confined to the soma (LS); middle: expression of plasticity confined to the region spanning 200–300 μm on the somato-apical trunk (LD); right: global expression of plasticity (GL; excluding the axon). Color-codes of the labels on the top of each neuron serve for interpretation of plots in (E–J). We increased I_h such that the maximal percentage change in $\bar{R}_{in}$ was 25–30%. The exact profile of changes required in $\bar{g}_h$ ((E); values of $\bar{g}_h$ are normalized with respect to the baseline profile in (B)) or $V_{1/2}$ ((H); values indicate depolarizing shifts to the activation kinetics with respect to baseline values) are shown for each of the three configurations in (D). It should be noted that the same percentage increase in $\bar{g}_h$, or the same depolarizing shift to $V_{1/2}$, would lead to a larger increase in dendritic I_h than in somatic I_h given the non-uniform baseline gradient in $\bar{g}_h$ (B). Irrespective of whether plasticity expresses as an increase in $\bar{g}_h$ (E–G) or a depolarizing shift of $V_{1/2}$ (H—J), a global increase in I_h (GL) is required to match experimental results (Fig. 4–5) on near-identical plasticity in f_R (F) & (I) and $\bar{R}_{in}$ (G) & (J) across the somato-apical trunk (see Fig. S14). Increase in I_h confined to the soma or a dendritic segment leads to local changes only around the soma ((F–G); LS) or around the dendritic segment ((F–G); LD), respectively. The requisite maximal percentage of 25% in input resistance, and a corresponding change in resonance frequency were not achievable by just shifting the activation kinetics in the LS and LD cases, owing to the bell-shaped dependence

of f_R on the $V_{1/2}$ of the activation kinetics (Fig. 7D and Fig. S13D) and the contribution of adjacent compartments to $\bar{R}_{in}$ and f_R measurements (Fig. S12). Consequently, the LS case is not shown in (I) & (J), while for the LD case, the maximum achievable plasticity in f_R (I) and $\bar{R}_{in}$ (J) are shown. It may be noted that this maximum achievable plasticity is still confined to the region of shift in the activation kinetics (LD; (I)).